G.A. Ashirova [ID] , A.O. Beketaeva[1] ,

A.Zh. Naimanova[1] [ID] ,V.V. Bykov[2] [ID]

[1]Institute of Mathematics and Mathematical Modeling, Almaty, Kazakhstan
[2]Karlsruhe Institute of Technology Institute of Technical Thermodynamics, Karlsruhe, Germany
*e-mail: ashirova@math.kz

Numerical study of flow structure (mixing process and reactivity) of diluted hydrogen non-premixed supersonic combustion system

Abstract. Numerical simulation of supersonic combustion with transverse hydrogen injection is performed by solving the three-dimensional Favre-averaged Navier–Stokes equations coupled by the $k - \omega$ turbulence model. These equations are solved using an algorithm that is based on the third-order essentially nonoscillatory scheme. Several cases of the jet compositions (pure hydrogen and hydrogen diluted by nitrogen in 50:50 mol%) are considered to study the influence of the composition onto the structure and reactivity of the supersonic combustion systems. Seven step modified version of Spark model developed by Jachimowski is implemented to model chemical reaction of hydrogen combustion, which performs quite well in the considered relatively high temperatures. The simulation revealed that the jet penetration heights are equal for both cases, and the hydrodynamic fields looked similar except for the temperatures of the zones located ahead and behind the jet injection. The chemical reaction zone, indicated by OH radicals, was more intense for the pure hydrogen case, occupying a narrow region along the oblique shock wave line. In contrast, the use of a hydrogen/nitrogen jet mixture resulted in a significantly wider flame front zone. This suggests that the presence of nitrogen in the mixture diluted the hydrogen concentration, leading to slower combustion. The study shows that the flow properties and reactivity of the mixture significantly changing with the dilutions of the fuel composition.
Key words: Supersonic combustion, hydrogen combustion, transverse injection, multicomponent gas, Navier - Stokes equations.

1. Introduction

The perpendicularly Jet in Cross-Flow (JICF) plays an important role in many technical applications, in industry (for example, industrial flare stack), in rocket propulsion systems. Many studies have been carried out to study the performance of this system at both essentially subsonic and supersonic flows, especially in non-reactive regimes. At supersonic flows, cross-flow jets have been used as a simple fuel delivery configuration in supersonic internal combustion engines [1-2] Various configurations of single or staggered nozzles have been proposed and studied as fuel delivery for air-breathing high-speed scramjet propulsion systems. Limitations in flame retention, penetration and mixing performance in these configurations have been identified and various strategies have been considered to improve mixing [3].

Figure 1 shows the flow structure in the plane of symmetry from [4-8]. When a supersonic flow impinges on the jet, the pressure in front of the jet increases due to flow deceleration, and a head shock occurs, (1 in Figure 1). An oblique shock wave 2 departs from it upstream, behind which, in addition to the separation zone, there is also a zone of supersonic flow. The subsequent deceleration of the flow is accompanied by the appearance of a second shock wave, the closing shock wave 3 parallel to the jet axis. As can be seen from the figure, the outgoing shock wave 1, the oblique shock wave 2, and the closing shock wave 3 intersect at one point and form a complex λ-shaped structure of shock waves 4. The pressure at the front boundary of the jet is not constant. It follows from the experiment [9] that its maximum value falls on the region beyond the point of intersection of shock waves, namely, the pressure maximum is located behind the lower part of the closing shock wave.
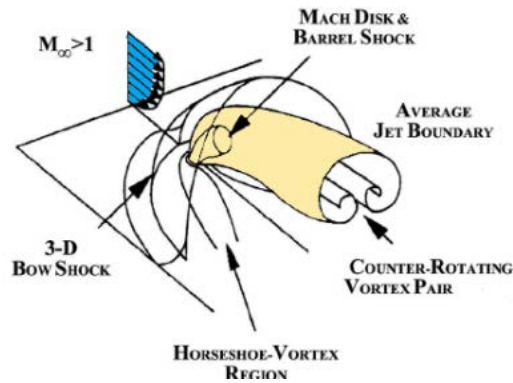
Figure 1 - Scheme of transverse gas injection (Gruber et al. [4])

It is known that the interaction properties of a transverse jet and flow are described by the ratio of the jet momentum to the flow momentum both for subsonic flows [10-11] and for the supersonic case [12]. This parameter expressed as the density of the jet multiplied by the square of the jet velocity, divided by the density of the crossflow multiplied by the square of the crossflow velocity. In particular, properties such as jet penetration height, velocity damping and concentration are assumed to scale only with the parameter J. This fact has been confirmed in experimental works in the supersonic flows represented e.g. in [13-14]. Therefore, according to this conclusion, two JISCFs with the same J value but different density ρ and velocity u values must be the same. In particular, they must have the same cross-jet penetration, which means they are subjected to the same mixing process. For example, the outflow of a light or heavy gas in such a way that the values of u (and hence ρ) are different, but the values of J are the same leads to the same structure of interaction with a supersonic transverse flow. At the same time, it must be said that less attention has been paid to reacting transverse jets in a supersonic air flow, partly because of the stringent requirements for the initiation and maintenance of combustion in a supersonic flow. Several studies, however, have focused on developing the ability to investigate the flow field of supersonic reactant streams [15-16] and to investigate the ignition characteristics of transverse hydrogen jets [17-21]. Moreover, the study of the effect of different compositions of the blown jet on the characteristics, mixing, and structure of these transverse jets in a supersonic transverse flow is rather limited, and the presented work is aimed at further study this subject.

Several cases of varying inflow jet compassions are considered, which have the same ratio of jet momentum of a transverse jet and flow such that the changing composition should not significantly change the flow structure and, thus, one can single out and investigate the influence of composition on the properties of chemical reaction and mixing within a supersonic combustion flow.

2. Mathematical models

2.1 Governing Equations

The dynamics of supersonic turbulent flow is described by the three-dimensional Favre-averaged Navier-Stokes equations of a compressible reacting multispecies gas mixture:

$$\frac{\partial \vec{U}}{\partial t} + \frac{\partial \left(\vec{E} - \vec{E}_v \right)}{\partial x} + \frac{\partial \left(\vec{F} - \vec{F}_v \right)}{\partial y} + \frac{\partial \left(\vec{G} - \vec{G}_v \right)}{\partial z} = \vec{S},$$ (1)

$$\vec{U} = \left(\rho, \rho u, \rho v, \rho w, E_t, \rho Y_i, \rho k, \rho \omega \right)^T,$$

$$\vec{E} = \left(\rho u, \rho u^2 + P, \rho uv, \rho uw, (E_t + P)u, \rho u Y_i, \rho uk, \rho u\omega \right)^T,$$

$$\vec{E}_v = \left(0, \tau_{xx}, \tau_{xy}, \tau_{xz}, u\tau_{xx} + v\tau_{xy} + w\tau_{xz} - q_x, J_{ix}, \frac{1}{\text{Re}}(\mu_l + \sigma_k\mu_t)\frac{\partial k}{\partial x}, \frac{1}{\text{Re}}(\mu_l + \sigma_\omega\mu)\frac{\partial \omega}{\partial x} \right)^T,$$

$$\vec{F} = \left(\rho v, \rho uv, \rho v^2 + P, \rho vw, (E_t + P)v, \rho v Y_i, \rho vk, \rho v\omega \right)^T,$$

$$\vec{F}_v = \left(0, \tau_{xy}, \tau_{yy}, \tau_{yz}, u\tau_{xy} + v\tau_{yy} + w\tau_{yz} - q_y, J_{iy}, \frac{1}{\text{Re}}(\mu_l + \sigma_k\mu_t)\frac{\partial k}{\partial y}, \frac{1}{\text{Re}}(\mu_l + \sigma_\omega\mu)\frac{\partial \omega}{\partial y} \right)^T,$$

$$\vec{G} = \left(\rho w, \rho uw, \rho vw, \rho w^2 + P, (E_t + P)w, \rho w Y_i, \rho wk, \rho w\omega \right)^T,$$

$$\vec{G}_v = \left(0, \tau_{xz}, \tau_{yz}, \tau_{zz}, u\tau_{xz} + v\tau_{yz} + w\tau_{zz} - q_z, J_{iz}, \frac{1}{\text{Re}}(\mu_l + \sigma_k\mu_t)\frac{\partial k}{\partial z}, \frac{1}{\text{Re}}(\mu_l + \sigma_\omega\mu)\frac{\partial \omega}{\partial z} \right)^T,$$

$$\vec{S} = \left(0, \quad 0, \quad 0, 0, 0, \overset{\bullet}{W}_k, (P_k - \beta^*\rho\omega k), (\gamma^*\rho P_k / \mu_t - \beta\rho\omega^2) \right)^T,$$

$$P = \frac{\rho T}{\gamma_\infty M_\infty^2 W}, W = \left(\sum_{k=1}^{N_p} \frac{Y_k}{W_k} \right)^{-1} \sum_{k=1}^{N_p} Y_k = 1, E_t = \frac{\rho}{\gamma_\infty M_\infty^2}h - P + \frac{1}{2}\rho(u^2 + w^2),$$

$$h = \sum_{k=1}^{N_p} Y_k h_k, h_k = h_k^0 + \int_{T_0}^{T} c_{pk}dT, c_{pk} = C_{pk} / W_k, C_{pk} = \sum_{i=1}^{5} \overline{a}_{ki}T^{(i-1)}, \overline{a}_{jk} = a_{jk}T_\infty^{j-1},$$

$$\tau_{xx} = \frac{2\mu_t}{3\text{Re}}(2u_x - v_y - w_z), \tau_{yy} = \frac{2\mu_t}{3\text{Re}}(2v_y - u_x - w_z), \tau_{zz} = \frac{2\mu_t}{3\text{Re}}(2w_z - u_x - v_y),$$

$$q_x = \left(\frac{\mu}{\text{Pr}\cdot\text{Re}} \right)\frac{\partial T}{\partial x} + \frac{1}{\gamma_\infty M_\infty^2}\sum_{k=1}^{N_p} h_k J_{xk}, q_y = \left(\frac{\mu}{\text{Pr}\cdot\text{Re}} \right)\frac{\partial T}{\partial y} + \frac{1}{\gamma_\infty M_\infty^2}\sum_{k=1}^{N_p} h_k J_{yk},$$

$$q_z = \left(\frac{\mu}{\text{Pr}\cdot\text{Re}} \right)\frac{\partial T}{\partial z} + \frac{1}{\gamma_\infty M_\infty^2}\sum_{k=1}^{N_p} h_k J_{zk}, J_{kx} = -\frac{\mu}{Sc\cdot\text{Re}}\frac{\partial Y_k}{\partial x}, J_{ky} = -\frac{\mu}{Sc\cdot\text{Re}}\frac{\partial Y_k}{\partial y}, J_{kz} = -\frac{\mu}{Sc\cdot\text{Re}}\frac{\partial Y_k}{\partial z},$$

$$\mu = \mu_l + \mu_t, \mu_l = \sum_{i=1}^{N} \frac{X_i\mu_i}{\Phi_i}, \mu_t = \text{Re}\frac{\overline{\rho}k}{\omega},$$

$$P_k = \mu_t \left[\left(\frac{\partial u_i}{\partial x_j} + \frac{\partial u_j}{\partial x_i} \right)\frac{\partial u_i}{\partial x_j} - \frac{2}{3}\left(\frac{\partial u_k}{\partial x_k} \right)^2 \right] - \frac{2}{3}\rho k\frac{\partial u_k}{\partial x_k}, i, j, k = 1, 2, 3,$$

$$\sigma_k = 0.5, \sigma_\omega = 0.5, \beta^* = 0.09, \beta = 0.075, \gamma^* = 5/9$$

Here, t is time; u, v, w are the flow velocity components in the x, y, z directions respectively; ρ is the density, T is the temperature, P is the pressure, E_t is the total energy, Y_k is the mass concentration of k component, $\tau_{xx}, \tau_{yy}, \tau_{zz}, \tau_{xz}, \tau_{xy}, \tau_{yz}$ are the viscous stress tensor; $q_x, q_y, q_z, J_{xk}, J_{yk}, J_{zk}$ are the thermal and the diffusive fluxes (diffusive fluxes are calculated by the Fick's law); c_v is the heat capacity at constant volume; γ is the adiabatic exponent; W

is molecular weight of mixture, $\dot{W}_k$ is the source term for mass fraction equations describing chemical reactions, M_∞ is the Mach number of the flow; subscripts "0" and "∞" will mark the jet and flow parameters, μ_t is the turbulent viscosity [22], and μ_l is laminar viscosity [23], k is the turbulent kinetic energy, ω is specific dissipation rate, P_k is the term defining the turbulence generation, Re, Pr, Sc are Reynolds, Prandtl and Schmidt numbers respectively.

Table 1 – H_2/air combustion mechanism (units: s, mole, cm³, cal, K) [25].

№	Reaction	A	b	T_a
1	$H_2 + O_2 \rightarrow OH + OH$	0.170E+14	0.0	24233
2	$H + O_2 \rightarrow OH + O$	0.142E+15	0.0	8254
3	$OH + H_2 \rightarrow H_2O + H$	0.316E+08	1.8	1525
4	$O + H_2 \rightarrow OH + H$	0.207E+15	0.0	6920
5	$OH + OH \rightarrow H_2O + O$	0.550E+14	0.0	3523
6	$H + OH + M \rightarrow H_2O + M$	0.221E+23	-2.0	0
7	$H + H + M \rightarrow H_2 + M$	0.653E+18	-1.0	0

The molar specific heats C_{pk} are determined from the experimental data by means of polynomial interpolation of the fourth order in temperature. Numerical values of empirical constants a_{jk} are taken from the table JANAF [24] at normal pressure ($p = 1\ atm$) and temperature $T^0 = 293\ K$.

The system of equations (1) is written in dimensionless form, the flow parameters $u_\infty, \rho_\infty, T_\infty, W_\infty$ are taken as reference values, for the pressure P and the total energy E_t the reference value are $\rho_\infty u_\infty^2$, for the specific enthalpy h_k are $R^0 T_\infty / W_\infty$, for the molar specific heats C_{pk} are R^0, and the radius of circular orifice of jet injection r_0 is chosen as the reference length scale.

2.2 Combustion model

The source terms for mass fraction equations describing chemical reactions are defined as:

$$\dot{\omega}_k = W_k \sum_{j=1}^{nr} \left(v'_{kj} - v''_{kj} \right) \omega_j \qquad (2)$$

Here W_k is the molecular weight of k component, v'_{kj} is the stoichiometric coefficient of the reactants, v''_{kj} is the stoichiometric coefficient of the products, nr is the total number of species involved.

The generalized law of mass action provides for the rates of individual chemical reactions

$$\omega_j = f_j \cdot \left(k_j^f \prod_{i=1}^{ns} \left(\rho \frac{Y_i}{W_i} \right)^{v'_{ij}} - k_j^b \prod_{i=1}^{ns} \left(\rho \frac{Y_i}{W_i} \right)^{v''_{ij}} \right)$$

Here ω_j is the mass reaction rate of kth species per unit volume. Index of mass concentration Y_k when $k = 1$ corresponds to H_2, $k = 2 - O_2$, $k = 3 - H_2O$, $k = 4 - OH$, $k = 5 - H$, $k = 6 - O$, $k = 7 - N_2$; $ns = 7$ is the number of components of gases.

To determine the rate of formation of the gas mixture component ω_j in the diffusion equation, it

is necessary to determine the chemical kinetics of the hydrogen-air mixture combustion. This requires a mechanism of chemical reactions. In this work, the abridged Spark chemistry model [25] (Tab.1) is considered. Six reacting species and an inert species N_2 participate in a 7-step mechanism (7-species/7-step). The expressions for forward reactions rate constants $k_j^f, j = 1, ..., 7$ are taken in the standard Arrhenius form:

$$k_j^f = A_j T^{\beta_j} \exp\left(-\frac{E_j}{RT}\right).$$

Here A_j is the pre-exponential factor, β_j is temperature exponent, E_j is the activation energy. Once provided and present the inverse reaction rate coefficients are defined via equilibrium constant:

$$k_j^b = \frac{k_j^f}{k_j^c(T)}$$

This way, the equilibrium constant k_j^c helps to determine the inverse reaction rate. This can be found using the Gibbs energies $\Delta G_j^0 = \frac{\Delta H_j}{T} - \Delta S_j$ of each component:

$$k_j^c = \left(\frac{1}{RT}\right)^{\Delta \nu_j} \exp\left(-\frac{\Delta G_j^0}{RT}\right)$$

Here

$$\Delta H_j = \sum_{i=1}^{m}\left(\nu_{ij}'' - \nu_{ij}'\right) \cdot H_i, \Delta S_j = \sum_{i=1}^{m}\left(\nu_{ij}'' - \nu_{ij}'\right) \cdot S_i,$$

and H_i, S_i – molar enthalpy and entropy of the i-th component, which can be determined from the JANAF table [24]. Consider separately the chemical reaction rates for each of the seven components

$$\omega_1 = D_1' \cdot \overline{k}_1^f \cdot \overline{\rho}^2 \cdot \left(\frac{Y_1}{W_1} \cdot \frac{Y_2}{W_2} - \frac{1}{\overline{k}_1^c}\left(\frac{Y_4}{W_4}\right)^2\right)$$

$$\omega_2 = D_2' \cdot \overline{k}_2^f \cdot \overline{\rho}^2 \cdot \left(\frac{Y_2}{W_2} \cdot \frac{Y_5}{W_5} - \frac{1}{\overline{k}_2^c}\frac{Y_4}{W_4}\frac{Y_6}{W_6}\right)$$

$$\omega_3 = D_3' \cdot \overline{k}_3^f \cdot \overline{\rho}^2 \cdot \left(\frac{Y_1}{W_1} \cdot \frac{Y_4}{W_4} - \frac{1}{\overline{k}_3^c}\frac{Y_3}{W_3}\frac{Y_5}{W_5}\right)$$

$$\omega_4 = D_4' \cdot \overline{k}_4^f \cdot \overline{\rho}^2 \cdot \left(\frac{Y_1}{W_1} \cdot \frac{Y_6}{W_6} - \frac{1}{\overline{k}_4^c}\frac{Y_4}{W_4}\frac{Y_5}{W_5}\right)$$

$$\omega_5 = D_5' \cdot \overline{k}_5^f \cdot \overline{\rho}^2 \cdot \left(\left(\frac{Y_4}{W_4}\right)^2 - \frac{1}{\overline{k}_5^c}\frac{Y_3}{W_3}\frac{Y_6}{W_6}\right)$$

$$\omega_6 = D_6'' \cdot \overline{k}_6^f \cdot \overline{\rho}^2 \left(\frac{Y_4}{W_4} \cdot \frac{Y_5}{W_5} - \frac{1}{\rho \overline{k}_6^c}\frac{Y_3}{W_3}\right) f_6^m$$

$$\omega_7 = D_7'' \cdot \overline{k}_7^f \cdot \overline{\rho}^2 \left(\left(\frac{Y_5}{W_5}\right)^2 - \frac{1}{\rho \overline{k}_7^c}\frac{Y_1}{W_1}\right) f_7^m$$

The sixth and seventh reactions, as shown in table 1, have a third body, M, which is modeled by the following expression:

$$f_j^m = \sum_{k=1}^{K} \alpha_{ki}\left(\rho \frac{Y_k}{W_k}\right), \quad j = 6, 7.$$

where collision coefficients / efficiencies are taken as $\alpha_{H_2} = 1$, $\alpha_{O_2} = 3.5$, $\alpha_{H_2O} = 6.5$, $\alpha_{OH} = 0$, $\alpha_H = 0$, $\alpha_O = 0$, $\alpha_{N_2} = 0.5$ respectively. Here ν_{ij}', ν_{ij}'' – stoichiometric coefficients of the forward and inverse j-th reaction, respectively; $\nu_{ij}'' < 0$, if the i component is considered in the j- reaction as a reagent, $\nu_{ij}'' > 0$ – as a product.

In dimensionless chemical reactions, there are two types of Damkohler numbers are introduced and used in the dimensionless form in the equations (1), namely,

$$D_i' = \frac{r_0}{u_\infty} \cdot A_i \cdot (T_\infty)^{\beta_i}\left(\frac{\rho_\infty}{W_\infty}\right); \quad i = 1, 2, 3, 4, 5,$$

$$D_i'' = \frac{r_0}{u_\infty} \cdot A_i \cdot (T_\infty)^{\beta_i} \cdot \left(\frac{\rho_\infty}{W_\infty}\right)^2; \quad i = 6, 7,$$

where the index i indicates the reaction number.

2.3 Initial and boundary conditions
The initial conditions coincide with the boundary conditions at the flowfield entrance.

– at the channel entrance

$$u = 1, \quad v = 0, \quad w = 0, \quad \rho = 1, \quad T = 1$$
$$x = 0, \quad 0 \le y \le H_y, \quad 0 \le z \le H_z$$

– on the lower wall,

$$u = 0, \quad v = 0, \quad w = 0, \quad \frac{\partial T}{\partial z} = 0, \quad \frac{\partial P}{\partial z} = 0,$$
$$z = 0, \quad 0 < x \le H_x, \quad 0 \le y \le H_y$$

At the entrance k, ω are determined using the Baldwin–Lomax algebraic model of turbulence on the base of the known averaged physical parameters of the free stream. Owing to the relation $P_k = \beta^* \rho \omega k$ the initial distribution of the turbulent parameters takes the form:

$$k = k_\infty, \text{ where } k_\infty = \frac{\mu_{tB-L}}{\rho \cdot \text{Re} \cdot \sqrt{\beta^*}} \sqrt{\frac{P_k}{\mu_{tB-L}}},$$

$$\omega = \omega_\infty, \text{ where } \omega_\infty = \frac{\rho k}{\mu_{tB-L} \cdot \text{Re}}.$$

The conditions for k and ω on the wall are

$$k = 0, \quad \omega = \frac{6\mu}{0.075 \rho (\Delta z_1)^2}$$

here Δz_1 - is the distance from the wall to the first node.

The boundary layer is given near to the wall too, where the longitudinal velocity component in the viscous sublayer [26] is determined by

$$u = 0.1 \left(\frac{z}{\delta_2} \right) + 0.9 \left(\frac{z}{\delta_2} \right)^2,$$

$$x = 0, \quad 0 \le y \le H_y, 0 \le z \le \delta_2,$$

where $\delta_2 = 0.1\delta_1$ is the viscous sublayer thickness [27], $\delta_1 = 0.37x (\text{Re}x)^{-0.2}$ is the boundary layer thickness [28].

In the turbulent boundary layer, the *1/7th* power law is used

$$u = \left(\frac{z}{\delta_1} \right)^{1/7}, \quad x = 0, \quad 0 \le y \le H_y, \delta_2 < z \le \delta_1$$

The profile of temperature and density values are taken as suggested and presented in [26]. The remaining boundary conditions are imposed in the following manner:

– the conditions at the entrance of the jet are

$$u = 0, \quad v = 0, \quad T = T_0, \quad w = \sqrt{T_0} \frac{M_0}{M_\infty},$$

$$z = 0, \quad \left| x^2 + y^2 \right| \le R$$

where $n = P_0 / P_\infty$ is the jet pressure ratio and M_0 is the jet Mach number.

– the condition of symmetry is imposed on the upper boundary

$$w = 0, \quad \frac{\partial u}{\partial z} = 0, \quad \frac{\partial v}{\partial z} = 0, \quad \frac{\partial T}{\partial z} = 0, \quad \frac{\partial k}{\partial z} = 0,$$

$$\frac{\partial \omega}{\partial z} = 0, \quad z = H_z, \quad 0 < x \le H_x, 0 \le y \le H_y$$

– the conditions on the side boundaries are

$$\frac{\partial u}{\partial y} = \frac{\partial v}{\partial y} = \frac{\partial w}{\partial y} = \frac{\partial \rho}{\partial y} = \frac{\partial k}{\partial y} = \frac{\partial \omega}{\partial y} = 0$$

$$y = 0, \quad y = H_y, \quad 0 < x \le H_x, \quad 0 \le z \le H_z$$

The NSCBC-like non-reflecting condition is imposed on the output boundary [29]. Here H_x, H_y, H_z are length, width and height of the computational domain, respectively, and R is the radius of the circular orifice.

2.4 Method of solution

The methodology of the numerical solution of the system of equations (1) can be found in [5, 26]. For the approximation of the convective terms, the ENO scheme of the third order is applied. The central differences of the second order of accuracy have been used for the approximation of the diffusion terms. The obtaining system of equations is solved by the factorization using the matrix sweep method for the vector of the thermodynamic parameters.
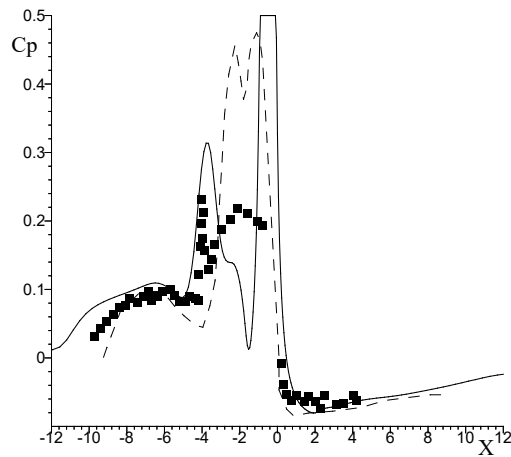
Figure 2 – Distribution of pressure coefficient C_p the symmetry axis

for $\mathrm{Re} = 1.87 \cdot 10^6$, $\mathrm{Pr} = 0.72$, $n = 282$, $M_0 = 1$, $M_\infty = 4$ «–» (solid curve) numerical results;

«■■■» (symbols) experiment [30]; and «---» (dashed curve) results obtained in [30].

The numerical calculations are performed with following parameters: the computational domain is $H_x = 20$, $H_y = 15$, $H_z = 10$ calibers, slot radius is $r_0 = 0.5$, the jet center is located at the point with the coordinates $x_0 = 10$, $y_0 = 7.5$. The calculations are performed on the grid $161 \times 101 \times 101$ with the steps over the spatial coordinates.

3. Results and Discussion

The comparison of the computational results with the experimental data [30] is performed for the problem of the supersonic turbulent airflow with transverse air jet injection for validation the numerical model. In Fig. 2, the numerical results for pressure coefficient C_p at the wall in the symmetry plane are compared with the results obtained in [30]. As can be seen, numerical results are in good agreement with experimental data.

Numerical simulations of supersonic combustion process using two different mixtures of fuel injected (pure hydrogen and hydrogen diluted 50:50 by nitrogen) as a transverse sound jet from bottom wall of the channel (see Fig. 1). A detailed comparison will be conducted between these two cases having different composite but same momentum ratio to ensure no much influences come from different supersonic flow interactions between streams.

The flow parameters are as following

$$M_\infty = 4, T_\infty = 1200 \ K, p_\infty = 10^6 \ Pa,$$

$$Y_{O_2} = 0.2221, \ Y_{N_2} = 0.7779,$$
$$\mathrm{Re} = 6.31 \cdot 10^4, \ \mathrm{Pr} = 0.9, Sc = 1, n = 15.61.$$

The hydrogen jet parameters are:

$$M_0 = 1, \ T_0 = 860.5 \ K, \ Y_{H_2} = 1.0.$$

The hydrogen/nitrogen jet parameters are:

$$M_0 = 1, \ T_0 = 800 \ K, \ Y_{H_2} = 0.5, \ Y_{N_2} = 0.5.$$

The parameters of the two jets are set up in a way that the momentum flux ratio is equivalent. The simulation is able to isolate the effects of the jet mixture composition on the flow behavior, mixing and combustion process by keeping same momentum flux ratio. The momentum flux ratio [1] is defined as

$$J = \frac{\rho_0 u_0^2}{\rho_\infty u_\infty^2},$$

where u_0 and u_∞ are jet and flow velocity respectively. The momentum flux ratio is $J = 1.02362$.
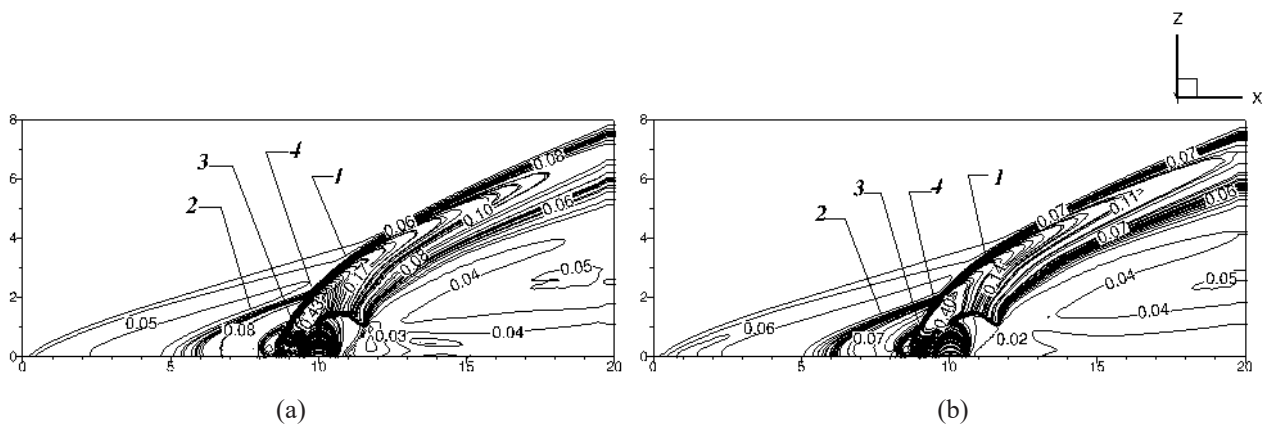
Figure 3 – Distribution of isobars in symmetry section, normal to y-axis in a) hydrogen jet, b) hydrogen/nitrogen jet.
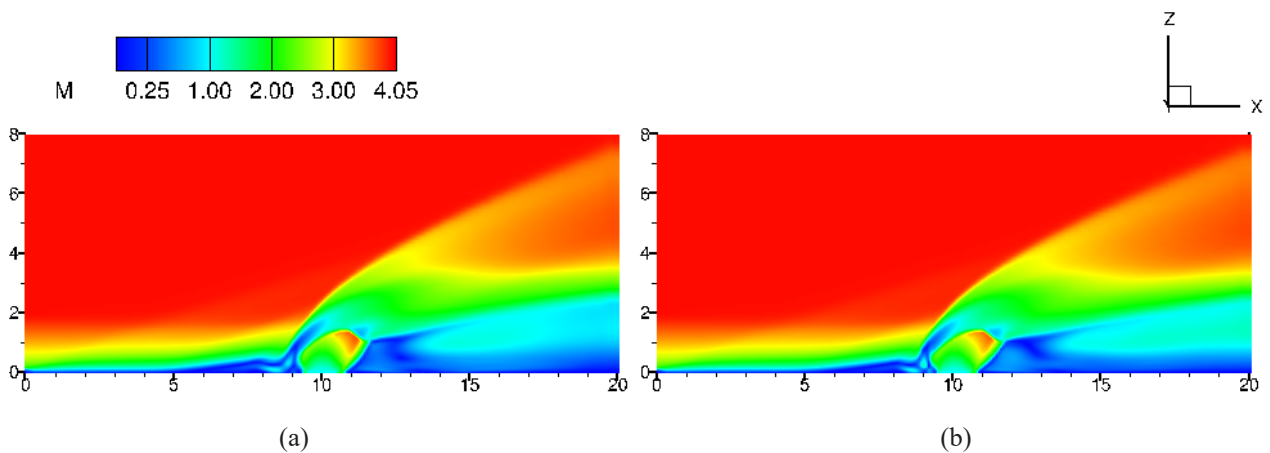
Figure 4 – Local Mach number distribution in symmetry section, normal
to y-axis in a) hydrogen jet, b) hydrogen/nitrogen jet.

The isobar levels / lines are shown in Fig. 3. The well-known and widely studied shock wave structure ahead of the jet injection is visible for two cases of fuel injection. It can be observed from Fig. 3(a) and 3(b) that the flow structures are the same because the momentum flux ratio is chosen to be equal.

The behavior of interaction between the jet and flow field are presented by the iso-Mach line contours in the jet injection region in Fig. 4. The identical jet penetration heights are revealed for both cases. The sonic jet accelerates as it penetrates into the high-speed cross-stream and becomes essentially supersonic. Then the supersonic zone is closed forming the barrel structure. Behind the Mach disk

the flow decelerates and becomes subsonic, and then the jet flow accelerates again to the main flow speed. The temperature distribution can be seen in Fig. 5 for two different jet mixtures. Because the rate of chemical reactions follows the Arrhenius equation, and thus, it is very sensitive to the temperature. Sharp changes in temperature occur in the region of formation of the λ- shock waves and subsonic zones due to the transverse jet injection, which creates an obstacle in the flow and additionally due to chemical reactions. The temperature values in these regions exceed the initial temperature of the jet and the flow. Increasing the temperature on shock waves promotes rapid combustion. In the region of intersection of the

jet with the main flow, the dimensionless temperature is approximately 2.5 (T=3000 K). This temperature is significantly higher than the initial maximum temperature of the main flow, which is 1200 K. Comparing Figs 5(a) and 5(b), it can be observed that temperature field is same except zones ahead and behind jet injection. In these zones temperature in case of hydrogen/nitrogen jet mixture is higher than in pure hydrogen jet mixture injection due to nitrogen presence. In spite of that, the maximum value of dimensionless temperature is equal 3.285 (T=3942 K). in both cases. This means the reaction takes plays and contributes to the energy of the system considerably. Though without much of differences between the cases with respect to the maximal values of the temperature.

(a)   (b)
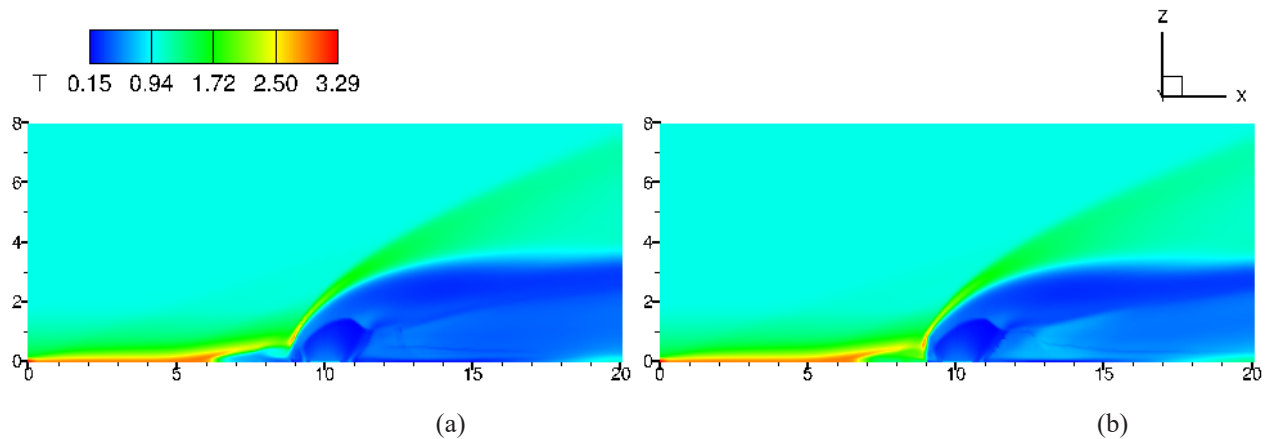
Figure 5 – Temperature distribution in symmetry section, normal to y-axis in a) hydrogen jet, b) hydrogen/nitrogen jet.

(a)   (b)
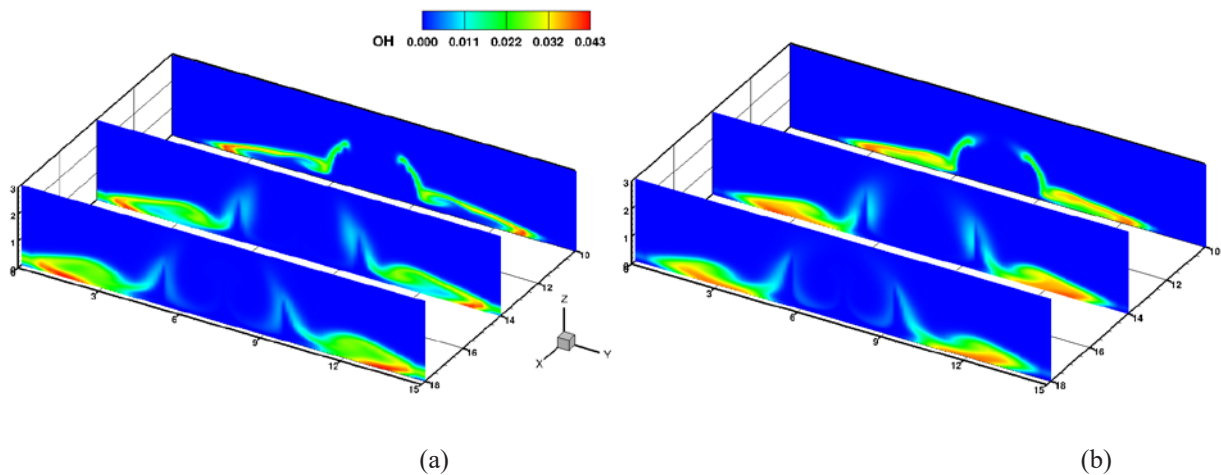
Figure 6 – Comparisons of the instantaneous OH distribution between (a)
hydrogen and (b) hydrogen/nitrogen jets at different planes (x/d = 10, 14 and 18).

The instantaneous OH distribution between hydrogen and hydrogen/nitrogen jets at different X planes (x/d = 10, 14 and 18) and the symmetry section Y with the plane section Z=0 are presented in Figs. 6 and 7. OH radical is frequently used as a reactive front indicator due to its significant role as an intermediate specie in chemical reactions. A bow shock forms ahead of each H_2 injector: the interaction between bow shocks and boundary layers leads to separation zones where H_2 recirculates. In these recirculation zones, OH radicals are produced, indicating that a flame already starts upstream of the

injectors and downstream of the flow separation. The peak value of OH mass fractions is approximately 0.0432 when hydrogen is used as the fuel. However, when the fuel mixture contains both hydrogen and nitrogen, the peak value of OH mass fractions is about 0.0400.

Figure 7 demonstrates further that the flame front has a wider profile when a hydrogen / nitrogen jet mixture is used, compared to a pure hydrogen jet mixture. In case of hydrogen jet mixture, Fig. 7(a) shows that the concentration of OH radicals is very low near the wall in the vicinity of the jet. In contrast, Fig. 7(b) of the second case indicates that OH radicals are mainly concentrated along the line of oblique shock wave.

Comparison of the instantaneous H_2O distribution between hydrogen and hydrogen/nitrogen jets at different X planes and the symmetry section Y with the plane section Z=0 is shown in Figs. 8 and 9 respectively. When hydrogen is used as the fuel in the combustion process, the peak value of H_2O mass fraction value observed is around 0.220.

(a)   (b)
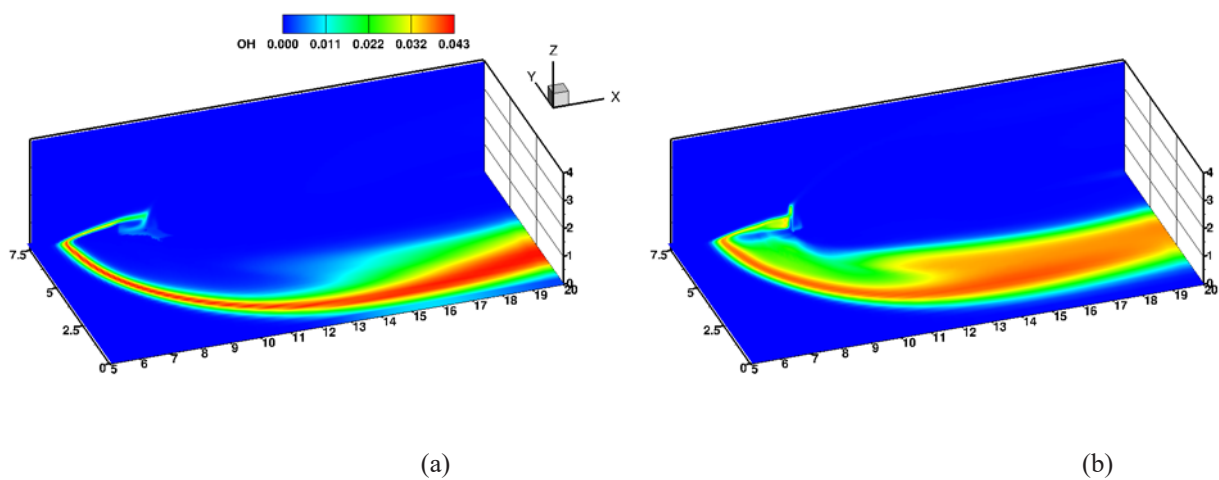
Figure 7 – The OH mass fraction in the symmetry section Y
with the plane section Z=0 in two cases: a) hydrogen jet and b) hydrogen/nitrogen jet.

(a)   (b)
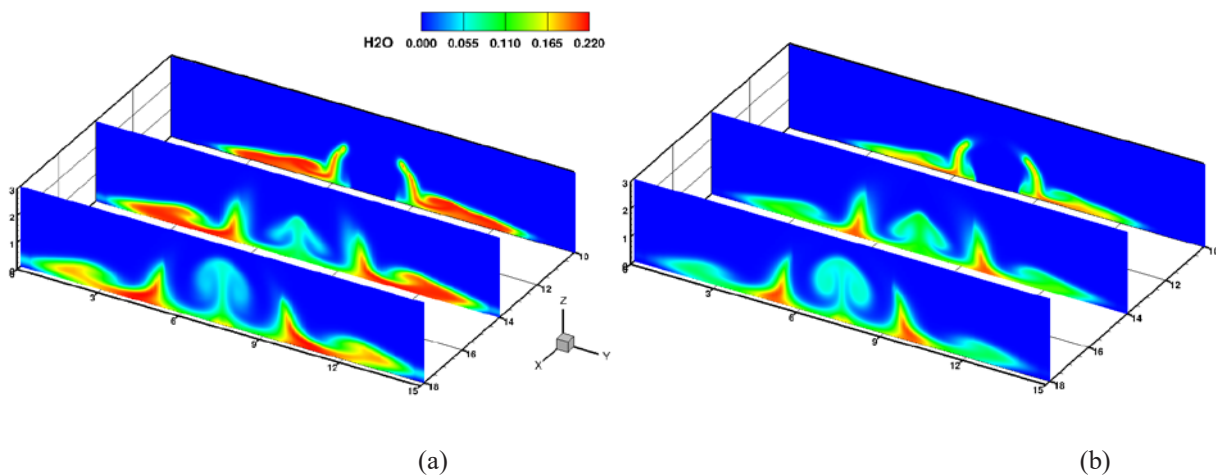
Figure 8 – Comparisons of the instantaneous H_2O distribution between (a)
hydrogen and (b) hydrogen/nitrogen jets at different planes (x/d = 10, 14 and 18).

(a)   (b)
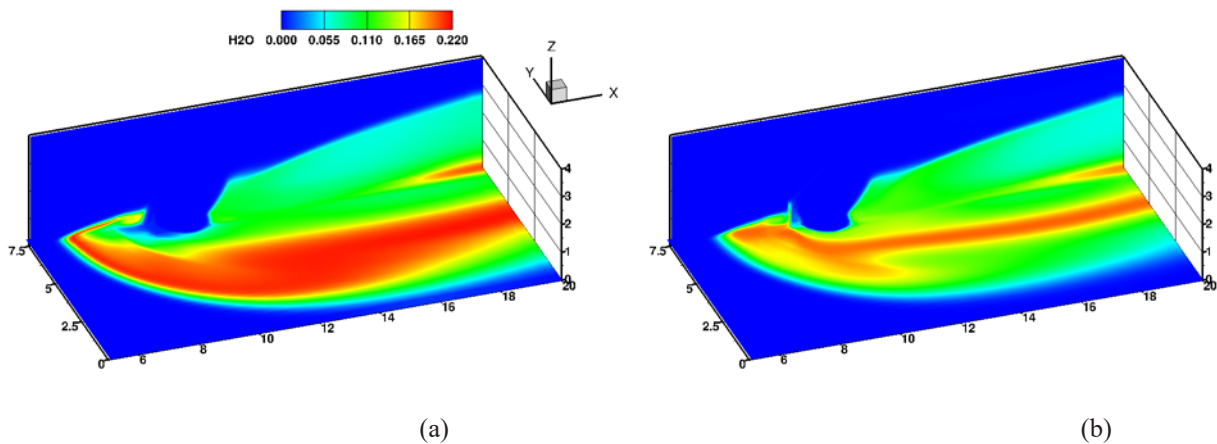
Figure 9. – The H_2O mass fraction in the symmetry section Y
with the plane section Z=0 in two cases: a) hydrogen jet and b) hydrogen/nitrogen jet.

On the other hand, if a mixture of hydrogen and nitrogen is used as fuel, maximum value observed for the H_2O mass fraction is 0.207.

Figures 9(a) and 9(b) show that distribution of H_2O mass fraction has similar structure but have significant differences in the quantity of water produced during the combustion process. It is visible from the Fig. 9(a) that, in the case of injection pure hydrogen jet mixture, the H_2O mass fractions on the wall are observed to reach

their maximum values in areas where OH mass fractions have very low values (as shown in Fig. 7(a)).

It can be seen that for both cases of jet mixture injected in supersonic airflow, see all Figs. 6-9, in regions where the OH mass concentration is disappeared, the water mass fractions are produced during the combustion process. It can be assumed based on the comparisons and observations made, which are presented in Figs. 6-9, that in case of injecting pure hydrogen jet in supersonic airflow the combustion process concentrates in a narrow regions and reaction zone looks sharper than in case of hydrogen/nitrogen jet. In the latter case the reaction zone looks broader and penetrates closer to the boundary layer, which signifies that the mixing process takes in the large domains, which can positively influence the completeness of combustion process.

To clarify this additional study both on reaction zone structure, mixing between streams as well on completeness of combustion process need to be

performed. This is the subject of ongoing our research and will be completed and published in the near future.

4. Conclusion

A numerical simulation of supersonic reactive flow with transverse jet injection in the channel is performed to compare the effect of two different jet mixtures - hydrogen and hydrogen/nitrogen - at the same momentum flux ratio - J. The simulation reveals that although the flow structure is similar in both cases, there are differences in the mixing, intensity and completeness of combustion processes.

The numerical results show as expected that the jet penetration heights are the same for both cases. Hydrodynamic fields (not a temperature) look also very similar. The small exception is observed for temperatures of the zones located ahead and behind jet injection. However, it is found that although the maximum temperature of the field is similar the chemical reaction, which is indicated by OH radicals, proceeds more intense for pure hydrogen case though it

occupies a narrow region near the wall in the vicinity of jet and mainly concentrated along the oblique shock wave line. The use of a hydrogen / nitrogen jet mixture results in a significantly wider flame front zone. It is revealed that injecting pure hydrogen jet into supersonic reactive airflow leads to a more rapid combustion process compared to injecting a hydrogen/nitrogen jet.

5. Funding

References

1. Gamba M., Miller V., Mungal M. G. "The reacting transverse jet in supersonic crossflow: physics and properties." In: 19th AIAA International Space Planes and Hypersonic Systems and Technologies Conference, 2014, P. 2014-3107.

2. Huber P. W., Schexnayder C. J., McClinton C. R. "Criteria for self-ignition of supersonic hydrogen-air mixtures." Tech. Report NASATP-1457, 1979.

3. Seiner J. M., Dash S. M., Kenzakowski D. C. Historical survey on enhanced mixing in scramjet engines // Journal of Propulsion and Power. -2001. - Vol. 17, No. 6. - P. 1273–1286.

4 Beketaeva A.O., Naimanova A. Zh. Flow structure of the transverse jet interaction with supersonic flow for moderate to high pressure ratios, // International Journal of Mechanics. – 2018. - Vol. 12. – P. 88-95.

5 Gruber M.R., Nejad A.S., Chen T.H., Dutton J.C. Transverse injection from circular and elliptic nozzles into a supersonic crossflow // Journal of Propulsion and Power. – 2000. – Vol. 16, № 3. – P. 449-457.

6 Beketaeva A. O., Bruel P., Naimanova A. Zh. Detailed Comparative Analysis of Interaction of a Supersonic Flow with a Transverse Gas Jet at High Pressure Ratios // Technical Physics. – 2019. - Vol. 64, № 10. – P. 1430 - 1440.

7 Beketaeva A.O., Moisseyeva Ye. S., Naimanova A. Zh. Numerical simulations of shock-wave interaction with a boundary layer in the plane supersonic flows with jet injection // Thermophysics and Aeromechanics. – 2016. - Vol. 23, № 2. – P. 173-183.

8 Beketaeva A. O., Naimanova, A. Zh., Shakhan N., Zadauly A. Simulation of the shock wave boundary layer interaction in flat channel with jet injection// ZAMM Zeitschrift fur Angewandte Mathematik und Mechanik – 2023. - P. 1-19

9 Glagolev A.I., Zubkov A.I., Panov Yu. A. Interaction of a gas jet flowing from a hole in a plate with a supersonic flow // Izvestiya AN SSSR. Mechanics of liquid and gas. - 1968. - No. 2. - P. 99-102.

10 Hasselbrink E. F., Mungal M. G. Transverse jets and jet flames. Part 1. Scaling laws for strong transverse jets // Journal Fluid Mechanics. – 2001. – Vol. 443.- P. 1–25.

11 Broadwell J. E., Breidenthal R. E. Structure and mixing of a transverse jet in incompressible flow // Fluid Mech. - 1984.- Vol. 148. – P. 405–412.

12 Schetz J. A., Billig F. S. Penetration of gaseous jets injected into a supersonic stream // Journal of Spacecraft and Rockets - 1966.- Vol 3, № 11. - P. 1658–1665.

13 Mahesh K. The interaction of jets with crossflow. // Annual Review of Fluid Mechanics. – 2013. – Vol. 45. – P. 379–407

14 Portz, R., Segal, C. Penetration of gaseous jets in supersonic flows // AIAA Journal. – 2006. – Vol. 44, № 10. – P. 2426–2429

15 McMillin B. K., Seitzman J. M., Hanson R. K. Comparison of NO and OH planar fluorescence temperature measurements in scramjet model flowfields. - AIAA Journal. – 1994.- Vol. 32, No. 10. - P. 1945–1952

16 Allen M. G., Parker T. E., Reineeke W. G., Legner H. H., Foutter R. R., Rawlins W. T., Davis S. J. Fluorescence imaging of OH and NO in a model supersonic combustor. – AIAA Journal. – 1993. - Vol. 31, No. 3. - P. 505–512

17 Ben-Yakar A., Hanson R. K. Experimental investigation of flame-holding capability of hydrogen transverse jet in supersonic crossflow // Proceedings of the Combustion Institute. – 1998. - Vol. 27. - P. 2173–2180.

18 Yoshida A., Tsuji H. Supersonic combustion of hydrogen in vitiated airstream using transverse injection // AIAA Journal. – 1977. - Vol. 15, No. 4.- P. 463–464

19 Rothstein A. D., Wantuck P. J. A study of normal injection of hydrogen into a heated supersonic flow using planar laser-induced fluorescence // AIAA Journal. – 2004. – P. 1992-3423.

20 Lee M. P., McMillin B. K., Palmer J. L., Hanson R. K. Planar fluorescence imaging of a transverse jet in a supersonic crossflow // AIAA Journal. – 1992.- Vol. 8, No. 4. - P. 729–735

21 Heltsley W. N., Snyder J. A., Cheung C. C., Mungal M. G., Hanson R. K. Combustion Stability Regimes of Hydrogen Jets in Supersonic Crossflow // 43rd AIAA/ASME/SAE/ASEE Joint Propulsion Conference & Exhibit. - 2007.

22 Wilcox D. C. "Turbulence modeling for CFD." DCW Industries Inc, USA, 2000, p. 537.

23 Лапин Ю.В., Стрелец М.Х. Внутренние течения газовых смесей. – М.: Наука, 1989. – 366 с.

24 Kee R.J., Rupley F.M., Miller J.A. "CHEMKIN-II: a Fortran chemical kinetic package for the analysis of gas-phase chemical kinetics." Sandia Report SAND89-8009B, 1989.

25 Eklund D., Drummond J. P., Hassan H.A. Calculation of supersonic turbulent reacting coaxial jets // AIAA Journal. - 1990. – Vol. 28, № 9.- P. 1633-1641

26 Beketaeva A., Bruel P., Naimanova A. Vortical structures behind a transverse jet in a super-sonic flow at high jet to crossflow pressure ratios // Journal of Applied Mechanics and Technical Physics. - 2015. - Vol. 56, No 5. - P. 777-788

27 Schlichting H. "Boundary-layer theory." McGraw-Hill, 1979.

28 Loytsyanskiy L. G. "Mechanics of liquids and gases." Pergamon Press, Oxford, 1966.

29 Poinsot T.J., Lele S. K. Boundary conditions for direct simulation of compressible viscous flows // Journal of Computational Physics. – 1992. -V. 101. - P. 104-129

30 Viti V., Neel R., Schetz J. Detailed Flow Physics of the Supersonic Jet Interaction Flow Field // Physics of Fluids. - 2009. - Vol. 21.- P.1-16.